

Turbidite emplacement on the southern Balearic Abyssal Plain (western Mediterranean Sea) during Marine Isotope Stages 1–3: an application of ITRAX XRF scanning of sediment cores to lithostratigraphic analysis

R. GUY ROTHWELL¹, BABETTE HOOGAKKER², JOHN THOMSON¹,
IAN W. CROUDACE¹ & MICHAEL FRENZ¹

¹*National Oceanography Centre, Empress Dock, Southampton SO14 3ZH, UK*

²*Department of Earth Sciences, University of Cambridge, Downing Street, Cambridge CB2 3EQ, UK*

Abstract: The upper part (0–20 m) of a long piston core from the SE Balearic Abyssal Plain – spanning the past 50 ka – has been studied using the ITRAX micro-XRF core scanner to obtain downcore elemental profiles. The Ca/Fe ratio was found to be an effective parameter to distinguish between turbidites and pelagites, because turbidites generally have higher Fe contents and lower Ca contents compared with pelagic intervals. Beds that were obscure when visually logged could be identified as turbidites or pelagites on their geochemical characteristics, allowing more complete subdivision of the sequence into genetic units. The ITRAX XRF data also provide useful information on textural grading, bioturbative mixing, identification of geochemically distinctive marker beds, indications of differences in provenance, and confirm or query the presence of early arrivals during turbidite emplacement. A chronostratigraphic framework for the core based on accelerator mass spectrometry (AMS) radiocarbon dating and correlation with oxygen isotope stages of pelagic intervals in other cores (using calcium carbonate stratigraphy) was also established. This shows that turbidite emplacement on this part of the Balearic Abyssal Plain has been modulated strongly by climate and sea-level change, with turbidite emplacement most frequent during the early Holocene when the rate of post-glacial sea-level rise was greatest. Deposition of the coarsest (i.e. sand and silt-based) turbidites at the core site was restricted to the full and Late Glacial (11–25 ka). Turbidite emplacement during Oxygen Isotope Stage 3 was rare. Most of the turbidites at the site are distal, but some coarse-grained-based turbidites are characterized by higher Sr/Ca ratios (possibly indicating a higher aragonite content), higher Ca and lower Fe contents compared to other turbidites, and are interpreted as having a more proximal shelf source. Such turbidites are generally rare, however, and restricted to full Glacial and Younger Dryas time. There is little evidence for large-scale seismogenic turbidites (expected to be seen as randomly timed emplacement, seemingly independent of eustatic control) at the core site, despite proximity to the seismically active Algerian margin 100 km to the south. This suggests that seismogenic turbidites must largely bypass this part of the plain. Although the ITRAX core scanner provides a rapid and non-destructive means of characterizing downcore geochemical distributions in great detail, interpretation of the data requires caution and assessment from an informed standpoint. Analytical artefacts such as those caused by water or organic content, degree of compaction, grain-size and mineral effects, unevenness of the cut core surface and poor discrimination of closely spaced element XRF peaks need identification and elimination.

The development of non-destructive X-ray fluorescence (XRF) instruments that scan cut sediment core sections to obtain high-resolution geochemical profiles has been a major technical advance for the study of sediment records. The first instrument for this type of analysis was the CORTEX XRF scanner developed by The Netherlands Institute for Sea Research, Texel, The Netherlands, and now marketed by Avaatech Analytical X-Ray Technology, Texel (Jansen

et al. 1998; Richter *et al.* 2006). Other XRF core scanners now available are the ITRAX micro-XRF core scanner with X-radiography, manufactured by Cox Analytical Systems of Gothenburg, Sweden (Croudace *et al.* 2006) and a high-resolution XRF core scanner made by Röntgenanalytik Messtechnik of Taunusstein, Germany (Haschke 2006). Most previous research using XRF core scanning has concentrated on palaeoceanographic studies (e.g.

Haug *et al.* 2001; Jahn *et al.* 2003; Kuhlmann *et al.* 2004; Lamy *et al.* 2004, and others). Relatively little work has been carried out on the application of continuous XRF profiling to deep-sea basin cores dominated by turbidites, which are typical of many marine basins, where the technique may have value in lithostratigraphic analysis and, perhaps, provenance studies.

Determination of genetic units (i.e. whether beds are autochthonous or allochthonous in origin) within cored sediment sequences is a fundamental prerequisite for lithostratigraphic and facies analysis, particularly for determining depositional processes and basin architecture. Identification of genetic units is necessary to determine depositional histories, estimate autochthonous and allochthonous sediment fluxes, and for investigation of the frequency of, and potential controls on, mass-wasting of continental margins. In marine basin sedimentary sequences, individual beds are commonly formed either through pelagic settling of material derived from biological surface productivity and wind-derived material through the water column (to form pelagites), or through advective sediment movement, usually involving sediment gravity flows, commonly turbidity currents that result in the deposition of turbidites. Turbidites are the distal products of downslope sediment transport and may form 90% of the basin-fill in some deep marine basins (Rothwell *et al.* 1992). Turbidites can be characterized on a sequence of textural characteristics that reflect gravitative particle settling within the waning flow (Bouma 1962; Stow & Shanmugam 1980; Lowe 1982). Traditional views hold that movement of terrigenous sediment to the deep sea by turbidity currents is greater at times of low sea level when rivers discharge their sediment loads closer to the shelf edge (e.g. Vail *et al.* 1977; Shanmugam & Moiola 1982, 1984; Posamentier & Vail 1988; Muto & Steel 2002). Some authors, however, suggest that sea-level change is an important factor in turbidite emplacement, and even that the rate of change of sea level is more important than low sea level in the generation of turbidites in aseismic areas (e.g. Weaver & Kuijpers 1983; Marjanac 1996).

Traditionally, the identification of turbidites in sediment sequences is based on a range of sedimentological and textural criteria, involving recording of visual descriptions of sedimentary structures and lithology, and specialized and sometimes time-consuming laboratory analyses such as grain-size determinations. Distinguishing turbidites in marine sediment cores can be straightforward if they show clear compositional, textural and colour differences from the

interbedded pelagites (e.g. Weaver & Rothwell 1987). Where the colour and texture of turbidites and pelagites are similar, however, for example where turbidites, derived from resuspension and downslope transport of pelagic sediment from topographic highs, pond in topographic lows or where both turbidites and pelagites are strongly coloured through hydrothermal staining (e.g. Rothwell *et al.* 1994), it may be difficult in practice to distinguish between pelagite and turbidite beds. Recognition may also be difficult when the turbidites are highly distal and consist entirely of mud, lacking textural features normally associated with graded bases. Further, it may be difficult to distinguish turbidite beds from pelagic layers if they are thin and extensively bioturbated. The presence of sharp bed bases and lack of obvious scattered foraminifers within the sediment (resulting in smooth structureless mud) are probably the best visual criteria for distinguishing turbidites from pelagic/hemipelagic muds. The upper few decimetres of turbidites are commonly bioturbated if the overlying sediment is pelagic or hemipelagic in origin. If bioturbation is moderate or intense, it can be difficult to ascertain the upper boundary of the turbidite bed with the overlying unit. This leads to difficulty in determining true thicknesses of pelagic/hemipelagic intervals and accurate assessment of pelagic accumulation rates and turbidite emplacement frequencies.

We report here a high-resolution geochemical and sedimentological study of the upper part of a long piston core from the SE Balearic Abyssal Plain in the western Mediterranean Sea. This core (LC06) was taken by the research vessel *Marion Dufresne* in 1995 in 2845 m water depth on the floor of the abyssal plain at 38°00.66'N and 7°11.09'E, 110 km north of Cap de Fer, Annaba, Algeria, which lies 400 km east of Algiers (Fig. 1). The core is 31 m in length, although we report here on the succession of the upper 20 m that spans the last 50 ka. We have sought to answer a number of questions relating to the usefulness of high-resolution XRF scanning in lithostratigraphic analysis and regarding the late Quaternary depositional history of this part of the Balearic Basin. Specifically:

- What are the best element or element ratio parameters, derived from high-resolution ITRAX scanning, for providing information on compositional contrasts, particle-size variation, provenance indications, diagenetic features and presence of exotic layers?
- Does variation in element profiles and sediment property profiles mirror textural and sedimentological parameters and enable

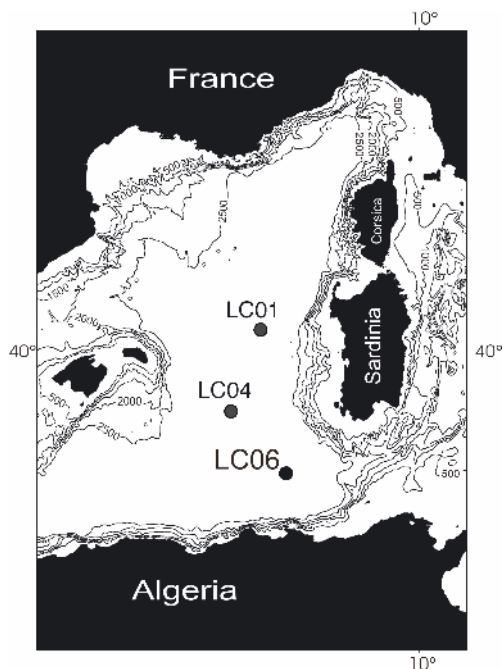


Fig. 1. Location of core LC06 on the Balearic Abyssal Plain in the western Mediterranean Sea. Position of comparator cores LC01 and LC04 are also shown. Bathymetric contour interval is 500 m.

better assessment of distality/proximality relationships?

- What has been the turbidite emplacement frequency, has this changed over time, and how has turbidite emplacement on this part of the abyssal plain been modulated by climate and sea-level change?

Methods

Core logging – discrimination of genetic units

Archive core sections from the upper 20 m of the sediment core were re-faced using glass slides and visually logged by conventional core description (Ocean Drilling Program 1987). Individual sediment units were identified as pelagites or turbidites on textural and sedimentological criteria, and where problematic (for example, where turbidites were thin and bioturbated throughout) using ITRAX-generated geochemical proxy data. Generally, turbidites were identified on the presence of burrowed upper boundaries, the absence of scattered foraminifers within mud intervals, the presence of sharp planar or eroded bases, and normally graded silty and/or sandy bases if

present. High Fe relative to Ca, indicative of the detrital clay to biogenic carbonate ratio, was an important indicator of Balearic plain turbidite intervals in the ITRAX data. Most turbidites are varying shades of olive green in colour, and some beds had paler green upper parts due to oxidation by bottom-water O_2 after emplacement (Wilson *et al.* 1986). Such dual-tone turbidites occur throughout the sequence studied, although some deeper turbidites show only one colour. Pelagic intervals were identified by colour (commonly pale fawn or brown) and the presence of scattered foraminifers and pteropod or shell debris throughout. Pelagic intervals commonly show slight–moderate bioturbation and burrowed lower boundaries. Sediment colour was measured using a Minolta CM-2002 spectrophotometer. Each section was independently logged by two of the authors (R.G. Rothwell and B. Hoogakker) with good agreement.

Dating of the sediment sequence

Three accelerator mass spectrometry (AMS) radiocarbon ages were available, determined on hand-picked planktonic foraminifera samples from pelagic intervals within the upper 20 m of this core (Table 1). The lowermost age (37 230 calibrated years BP) was disregarded as this is now believed to have been taken from a turbidite rather than a pelagic interval, so that the foraminifers analysed may have been derived from older deposits.

Hoogakker (2003) demonstrated that the calcium carbonate stratigraphy of pelagic records from the Balearic Abyssal Plain closely mirror the oxygen isotope record, with high $CaCO_3$ contents when planktonic foraminifera $\delta^{18}O$ values are low. Variation in pelagic calcium carbonate can therefore be used as a proxy to identify known oxygen isotope events. Measurement of the calcium carbonate contents of all pelagic intervals identified in core LC06 was made by coulometry. Samples were oven dried at 100 °C for 48 h, the dried samples were ground and $CaCO_3$ content measured from CO_2 liberated by addition of 10% phosphoric acid after 6 min (Hoogakker 2003). The resulting calcium carbonate stratigraphy of core LC06 was compared with those obtained from pelagic intervals in two other long piston cores from the Balearic Abyssal Plain (LC01, 40°15.82'N, 6°53.23'E, water depth 2845 m; and LC04, 38°39.01'N, 6°06.64'E, water depth 2800 m) both within 250 km of the LC06 core site (Figs 1 & 2). These cores had been calibrated by oxygen isotope measurements and this allowed identification of dated oxygen isotope events in LC06

Table 1. Absolute dates for pelagic intervals in core LC06

Depth (mbct)	Date type	¹⁴ C age years BP ±1 SD	Calibrated age (years BP)	Age model	Source
3.66–3.69*	AMS radiocarbon	7991 ± 43	8381–8481	8400	Hoogakker (2003)
13.46–13.65*	AMS radiocarbon	17730 ± 190	20 126–20 889	20 500	Rothwell <i>et al.</i> (1998)
19.17–19.19*	AMS radiocarbon	34380 ± 660	<i>c.</i> 37 230 [†]	<i>c.</i> 37 230	Rothwell <i>et al.</i> (1998)
19.87	Oxygen Isotope Event 3.3 [‡]	–	–	50 210	Hoogakker (2003)
20.46	Oxygen Isotope Event 3.31 [‡]	–	–	55 450	Hoogakker (2003)

* Depth in metres below core top is given as 1 m less than in the source works as we discount the uppermost 1 m core section (core section 31), which was empty and count core top as the top of core section 2. In the source works, the empty uppermost core section was included in depth calculations.

[†] Calibrated using the magnetic curve of Laj *et al.* (1996), other radiocarbon dates calibrated using INTCAL98 (Stuiver *et al.* 1998).

[‡] Inferred from calcium carbonate stratigraphy (see text).

(Table 1). The oxygen isotope analyses were made on hand-picked, consistently sized specimens of the foraminifer *Neogloboquadrina pachyderma* (dextral variety) using a Europa GEO 2020 stable isotope ratio mass spectrometer with individual acid-bath carbonate preparation (Hoogakker 2003).

Identification of these absolute age tie points within the pelagic record of LC06 allowed individual turbidites, identified through logging, to be dated to an approximate emplacement time. This was done through estimation of pelagic sedimentation rates between the tie points and consideration of the thickness of pelagic intervals between individual turbidites.

Element profiling using the ITRAX high-resolution XRF core scanner

Archive core sections covering the uppermost 20 m (0–50 ka BP, based on the dating evidence above) of core LC06 were run through the ITRAX micro-XRF core scanner. This instrument is designed to undertake high-resolution energy-dispersive XRF (ED-XRF) measurements along the longitudinal axis of split sediment cores. An optical image of the full split core surface and a 20 mm-wide continuous high-resolution X-radiograph are also obtained using optical and radiographic line cameras. The X-rays used to irradiate the core section are generated from a 3 kW Mo target and focused through a flat glass capillary waveguide to allow very high-resolution measurement (down to 200 µm step size). The X-ray dwell time (for X-radiography), count time (for XRF) and measurement step size are all user definable. Each ED-XRF spectrum is recorded and deconvolved to derive peak area integrals for indi-

vidual elements that are nominally proportional to concentrations of major and minor elements within the sediment. Elements can be detected in the range from Si to U. A more detailed description of the ITRAX instrument and the data generated is provided by Croudace *et al.* (2006).

In the present study, the selected step size was 0.5 mm with a XRF count time at each step of 30 s. Data for Al, Si, Ca, K, Ti, V, Mn, Fe, Ni, Cu, Zn, As, Br, Rb, Sr, and Zr are deconvolved from the X-ray spectra as the core runs through the ITRAX (elements lighter than Al currently cannot be measured using the ITRAX). In total, 40 000 XRF spectra over 20 m of core were collected, providing a uniquely detailed geochemical characterization of part of a deep-sea long piston core. The resulting XRF element

Fig. 2. Graphic logs (left) for cores LC01, LC04 and LC06. Turbidite intervals are shown as grey, pelagic intervals as black bands. The pelagic intervals are then summed to give total pelagic thickness (second column), which is then expanded by a factor of 8 to give 'Pelagic depth' (third column). This represents the pelagic sequence if no turbidites had been emplaced. Nannofossils zones for the pelagic sequence according to the scheme of Weaver (1983) are shown in column 4. The boundary between nannofossil zones 1 and 2 is dated to *c.* 50,000 years BP. Calcium carbonate profiles, derived through coulometry, for each core are shown together with oxygen isotope measurements for cores LC01 and LC04. Note the correlation between the calcium carbonate values and the oxygen isotope measurements in LC01 and LC04, showing the calcium carbonate stratigraphy to be a good proxy for oxygen isotope stages that can be used by analogy in core LC06. Emplacement of turbidites appears to cause little or no erosion of substrates. Position and dates of AMS radiocarbon dates are also shown.

peak integrals are summarized and stored as .txt files that can be visualized and manipulated either in Excel or Itrax.PLOT – a custom-built program developed by Southampton Oceanography Centre and JF Computing (Stanford in the Vale, Oxfordshire, UK). Aluminium is at the limit of ITRAX detection and counts for this element are low. Therefore we could not use Al as a reference element and had to find an alternative detrital divisor element for normalization purposes.

Grain-size analysis

To test whether variation in element ratio profiles determined by ITRAX XRF measurement mirrored textural parameters, one core section was analysed for grain size at 1 cm resolution. The grain-size analyses were carried out using a Malvern Mastersizer 2000 in combination with a Malvern Hydro G accessory unit and a 36-pot Malvern auto-sampler. This instrument is capable of analysing a size range from 0.02 to 2000 μm . Approximately 0.25 (if mud) to 1 cm^3 (if sand) of bulk sediment was taken and dispersed in a 0.05% sodium polyphosphate (Calgon) solution by shaking overnight. For the analyses, a laser-target obscuration (sample concentration) of 10–20% was selected. Settings of particle refractive index to 1.52 and an absorption value of 0.1 provide average values for mixed mineral assemblage of marine sediments. Three measurements were carried out on each sample for which the averages were calculated and exported in 0.2 phi steps to calculate the arithmetic mean grain size according to Krumbain (1936).

Results and discussion

A graphic log of the lithology of the upper 20 m of core LC06, derived from visual logging and ITRAX-measured geochemical proxies (principally the Ca/Fe ratio), is presented as Figure 3. A total of 52 turbidite beds were identified above the inferred depth for Oxygen Isotope Event 3.3 (indirectly dated at 50210 years BP; Martinson *et al.* 1987), which occurs at a depth of 19.87 metres below core top (mbct), giving an overall turbidite emplacement frequency of approximately one event every 960 years. Emplacement frequency has varied significantly over this time interval, however. Individual turbidites vary between less than 1 to 555 cm in thickness, and most turbidites consist of Te division mud (Bouma 1962) or graded–ungraded T6–T8 muds (Stow & Shanmugam 1980). Beds

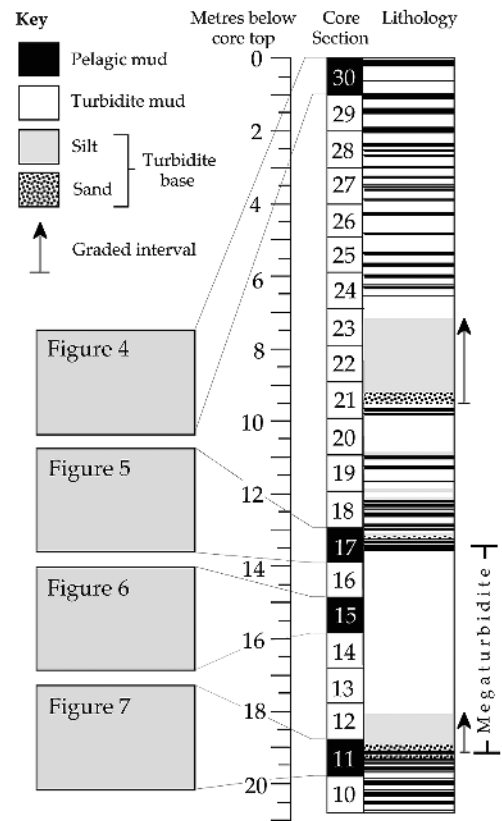


Fig. 3. Graphic log of the upper 20 m of core LC06 derived from visual and ITRAX logging. Beds are identified as pelagic or turbiditic in origin according to criteria described in the text. Core sections with illustrated XRF profiles are indicated. The megaturbidite is a large-volume deposit of basinwide extent, emplaced at 22 ka, during the last lowstand in sea level (Rothwell *et al.* 1998). Graded bases are indicated with arrows representing direction of fining.

with silty or sandy bases are generally rare and make up only about 15% of the total. Turbidites with basal sands make up 8% of the total. Turbidites with visibly coarser-grained bases, whether silt and/or sand, only occur between 5.90 and 19.26 mbct. Lamination is not seen in the coarser-grained bases, which commonly appear as massive, poorly sorted, normally graded sands and silts.

The response of the ITRAX core scanner to different element concentrations is variable as is normally the case with XRF analysis. The magnitude of element integrals depends mostly on excitation efficiency produced by the particular X-ray tube primary radiation (in this case a Mo tube), the energy of the elemental X-rays and

abundance of the element. For excitation of the sediments studied, Ca, Fe and Sr provide a good response, with K, Rb, Ti, Mn, As and Zn providing a moderate response. Br, Ni and Co can also provide useful information in organic-rich sediments (Thomson *et al.* 2006). A clear distinction in pelagite/turbidite beds in LC06 is shown from plots of Ca/Fe. Visual logging identified a small number of thin (<10 cm) heavily bioturbated beds of uncertain affinity. These lacked the sharp bases characteristic of turbidites, although patchy olive green colour and blebs of homogenous mud within these intervals suggested they may be thin turbidites bioturbated throughout their entire thickness. Examination of Ca/Fe ratios confirms this interpretation, showing Fe enrichment in all cases and enabling complete division of the sequence into genetic units, something that could not be done confidently on visual logging evidence alone.

Element concentrations are commonly expressed as ratios to a detrital phase element to avoid closed sum effects due to variations in calcium carbonate content, which will automatically cause variations in element profile integrals (Rollinson 1993; van der Weijden 2002). Usually elements are normalized to Al, but as this element is at the limit of ITRAX measurement an alternative element divisor characteristic of the detrital phase was needed. Figure 4 shows profiles for MoK Compton scattering (the magnitude inversely relating to mean atomic number), Fe/Al, Fe/Ti, Fe/K, Fe/Rb and other ratios through LC06 section 30. In this section, two turbidites, at 120–590 and 590–960 mm below section top, directly overlie one another. Compton scattering relates inversely to sediment mean atomic number so that atomic number increases where Compton scattering decreases. Visual logging recorded 2 mm of silt at 590 mm, but above this the unit appears as uniform homogenous olive green mud. Compton scattering decreases over a much longer interval (500–590 mm), revealing compositional grading not evident to the eye. Corresponding grading is not very obvious in the Fe/Ti ratio, except as a slight increase in Ti. A discrete peak at 380 mm, coincident with a narrow but conspicuous peak on the As integral profile, may indicate pyrite authigenesis. We consider K an unreliable divisor element as increases in K may relate to higher water content, as Cl from sea-water salt absorbs potassium K X-rays (Croudace *et al.* 2006). Rubidium typically shows a good signal on the ITRAX, and the Fe/Rb ratio shows the grading between 500 and 590 mm in the upper turbidite bed, seen as decreased Compton scattering values. We therefore consider Rb to be an

effective element divisor in the absence of precise Al, and this element was used in this study.

Element integral ratios or integrals that we believe likely to be the most informative in aiding sedimentological study or lithostratigraphic analysis are summarized in Table 2 together with their sensitivity to ITRAX detection and indicator properties. We present these element ratios plotted against lithology for three representative core sections from core LC06 (Figs 5–7). These figures include core photographs, X-radiographs and profiles for Compton scattering, Ca/Fe, Sr/Ca, Fe/Rb, K/Rb, Ti/Rb, Zr/Rb, Cu/Rb, As and Si profiles throughout core sections 17 (12.91–13.78 mbct), 15 (14.78–15.78 mbct) and 11 (18.78–19.78 mbct). These figures illustrate the range of trends seen in these element ratios and the Compton, As and Si integrals. Lithology determined by visual logging and the geochemical profiles is also shown. The geochemical plots confirm the lithological subdivision showing clear 'steps' or inflections at bed boundaries, although bioturbative mixing leads to gradational profiles in the upper parts of turbidite beds. Section 15 (Fig. 6) consists entirely of ungraded homogenous mud and comes from the mud interval of a very thick (5.5 m) sand-based megaturbidite previously identified by Rothwell *et al.* (1998) as a large-volume last glacial lowstand deposit of basin-wide extent. The Mo Compton scattering and element ratio profiles show its uniform nature. Below we offer observations on the parameters measured by the ITRAX and their significance.

Measured integrals and ratios

Compton scattering. The Compton scattering integral, which relates inversely to mean atomic number, decreases in the silt and sand layers due to size/density-related mineral fractionation. Grading, presumably due to mineralogical variation, can be also seen in this parameter, even when not visually obvious. Inflections in the profiles often correlate with bed boundaries. Sharp decreases in Compton scattering also correlate with discrete pteropod layers (e.g. Section 11, 79 cm, Fig. 7), possibly produced by current winnowing, as mean atomic number falls with looser sediment packing.

Ca/Fe ratio. The Ca/Fe ratio reflects carbonate content and in core LC06 generally shows a strong correlation to sedimentary units. In general, turbidite sands, silts and muds, presumably sourced from shallower water, are richer in Fe and poorer in Ca than pelagic interbeds. The

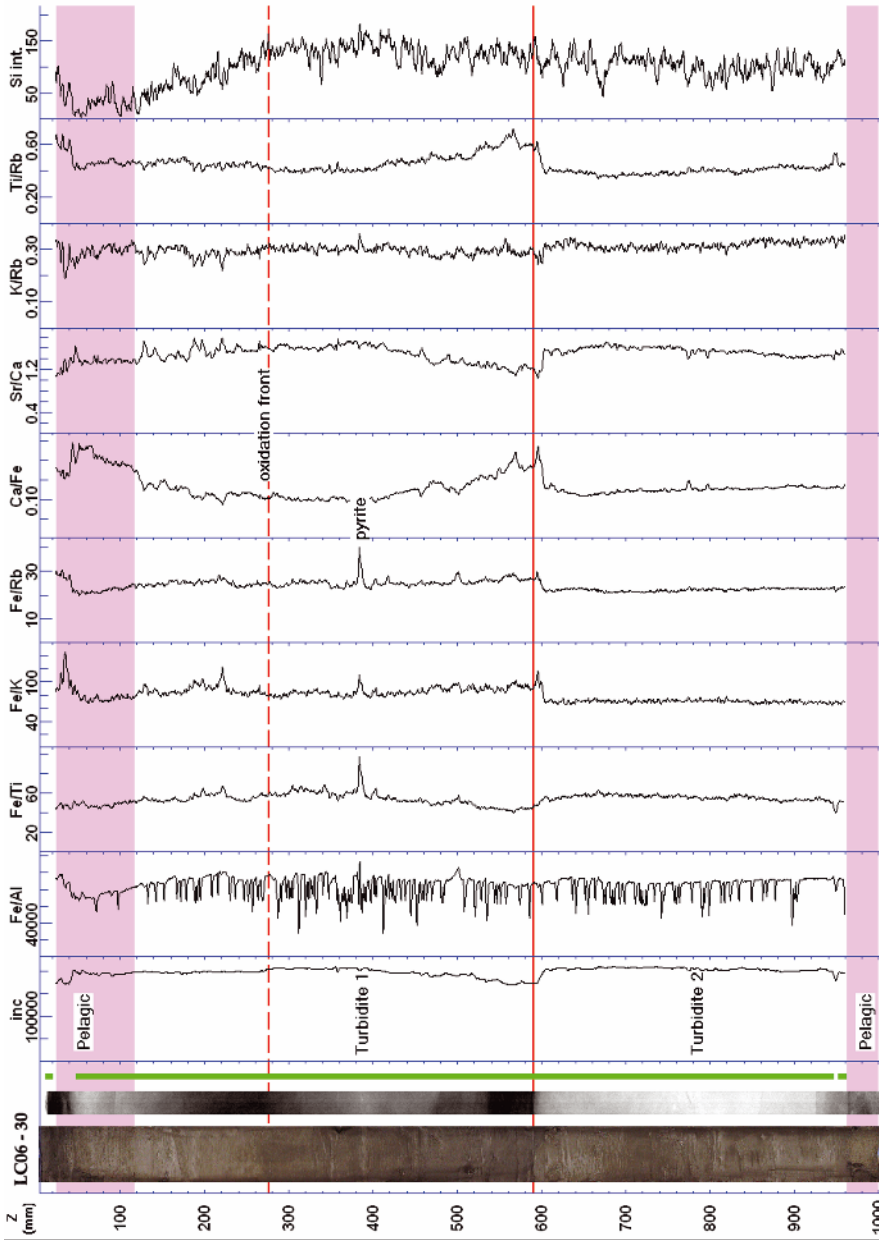


Fig. 4. Compton scattering (inc), Fe/Al, Fe/Ti, Fe/K and Fe/Rb ratios through LC06 section 30 (0–1.00 mbct). Ca/Fe, Sr/Ca, K/Rb, Ti/Rb ratios and Si profile are also shown. Pelagic intervals are indicated by solid mauve coloration and turbidites are white (unornamented). An oxidation front marked by a colour change within the upper part of Turbidite 1 (upper turbidite) is marked by dashed red line. A continuous red line represents the base of the turbidite. As aluminium is at the limit of ITRAX measurement, its use as a detrital divisor results in a poorly defined profile (Fe/Al). Rb is a more suitable element for normalization. Note grading in the base of Turbidite 1 evident from the Compton scattering profile (inc), which is mostly imperceptible to the naked eye, is apparent in the Ca/Fe and Ti/Rb ratios, but not in the Si profile.

Table 2. Property, element ratios or integrals believed to be informative in aiding sedimentological or lithostratigraphic analysis in clayey, sandy and carbonate-rich marine sediments together with their sensitivity to ITRAX detection (using a Mo X-ray tube) and indicator properties

Property, element ratio or integral	Sensitivity to ITRAX detection	Indicator properties
Compton scattering	High	<ul style="list-style-type: none"> • Relates inversely to mean atomic number, commonly decreases in silt and sand layers due to size/density-related mineral fractionation • May show grading due to mineralogical variation • Inflections in profile commonly correlate with bed boundaries • Mean atomic number falls with looser sediment packing, so winnowing of sediment may be seen as decreased Compton scattering
Ca/Fe	High	<ul style="list-style-type: none"> • Indicative of biogenic carbonate:detrital clay ratio • May show strong correlation with sedimentary units • Turbidites sourced from shallow water tend to be richer in Fe and poorer in Ca than pelagic interbeds • Ca/Fe profile is a good proxy for sediment grading, for identifying textural subdivisions within turbidites and for assessing source distality–proximality relationships • Ca/Fe profile within pelagites typically more variable than in turbidites, reflecting more heterogeneous sediment fabric • Ca peaks or their absence (commonly associated with increased Si) within turbidite bases distinguish foraminifer- or shell-rich and more terrigenous quartz-rich bases
Sr/Ca	High	<ul style="list-style-type: none"> • Enhanced Sr may indicate presence of high-Sr aragonite which requires a shallow-water source • Affected by sediment packing/porosity and grain-size/shape variations
Fe/Rb	Good	<ul style="list-style-type: none"> • Commonly shows grain-size related fractionation effects within turbidites • Fe mobilized during redox-related diagenesis and elevated Fe commonly seen in oxic, or formerly oxic, parts of turbidites • Rb is an element commonly associated with detrital clay and may be enhanced in turbidite muds
K/Rb	Moderate	<ul style="list-style-type: none"> • K is commonly associated with detrital clay and may be enhanced in turbidite muds • Unreliable parameter as sea-water Cl absorbs potassium X-rays, so apparent high K may reflect increased porosity
Zr/Rb Ti/Rb	Moderate	<ul style="list-style-type: none"> • Zr and Ti high in heavy resistate minerals and may be enhanced in turbidite bases • Sediment source/provenance indicators
Cu/Rb	Moderate	<ul style="list-style-type: none"> • Behaviour of Cu poorly understood but Cu peaks largely of diagenetic origin
As	Moderate	<ul style="list-style-type: none"> • Commonly an indicator of pyrite which may be detrital or authigenic in origin
Br/Cl	Moderate–low	<ul style="list-style-type: none"> • Indicator of organic-rich layers as Br high in organic-rich sediments. For marine sediments a constant ratio implies sea-water ratio
Si	Moderate–low	<ul style="list-style-type: none"> • Important terrigenous or productivity indicator • Normalization using detrital divisor can distinguish terrigenous or productivity origin • When terrigenous, useful as a sediment source and perhaps provenance indicator

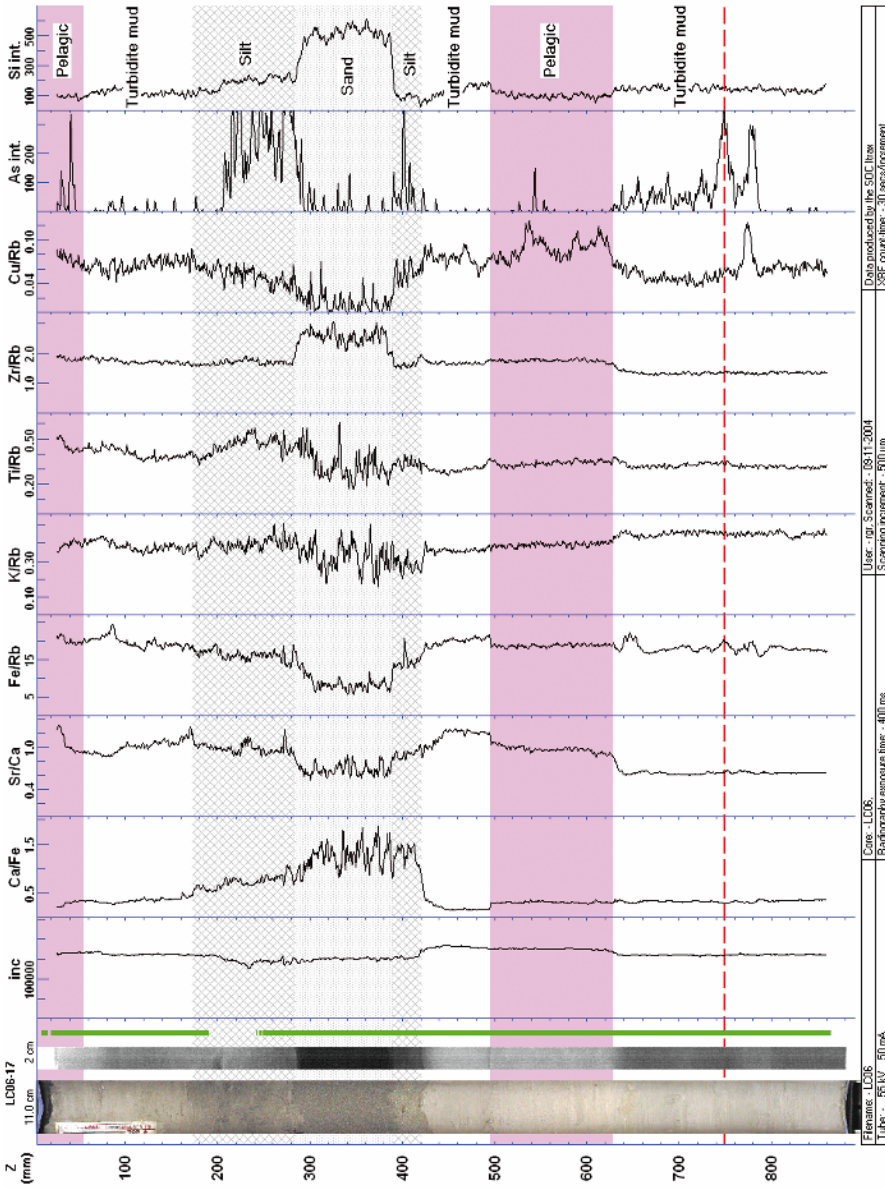


Fig. 5. Compton scattering and downcore geochemical profiles through LC06 Section 17 (12.91–13.78 mbct). A photograph of the split-core section together with a 2 cm-wide continuous X-radiograph from the centre of the 11 cm-wide core is shown to the left. The adjacent green line indicates data validity, and shows when the X-ray detector was in the correct position at a constant distance from the sediment surface (green) or was out of position (blank). Pelagic intervals are coloured mauve, sand is indicated by closed stipple, and silt by oblique cross-hatchures. White intervals are turbidite mud. An oxidation front, marked by a colour change within a turbidite at 750 mm, is shown by the red broken line.

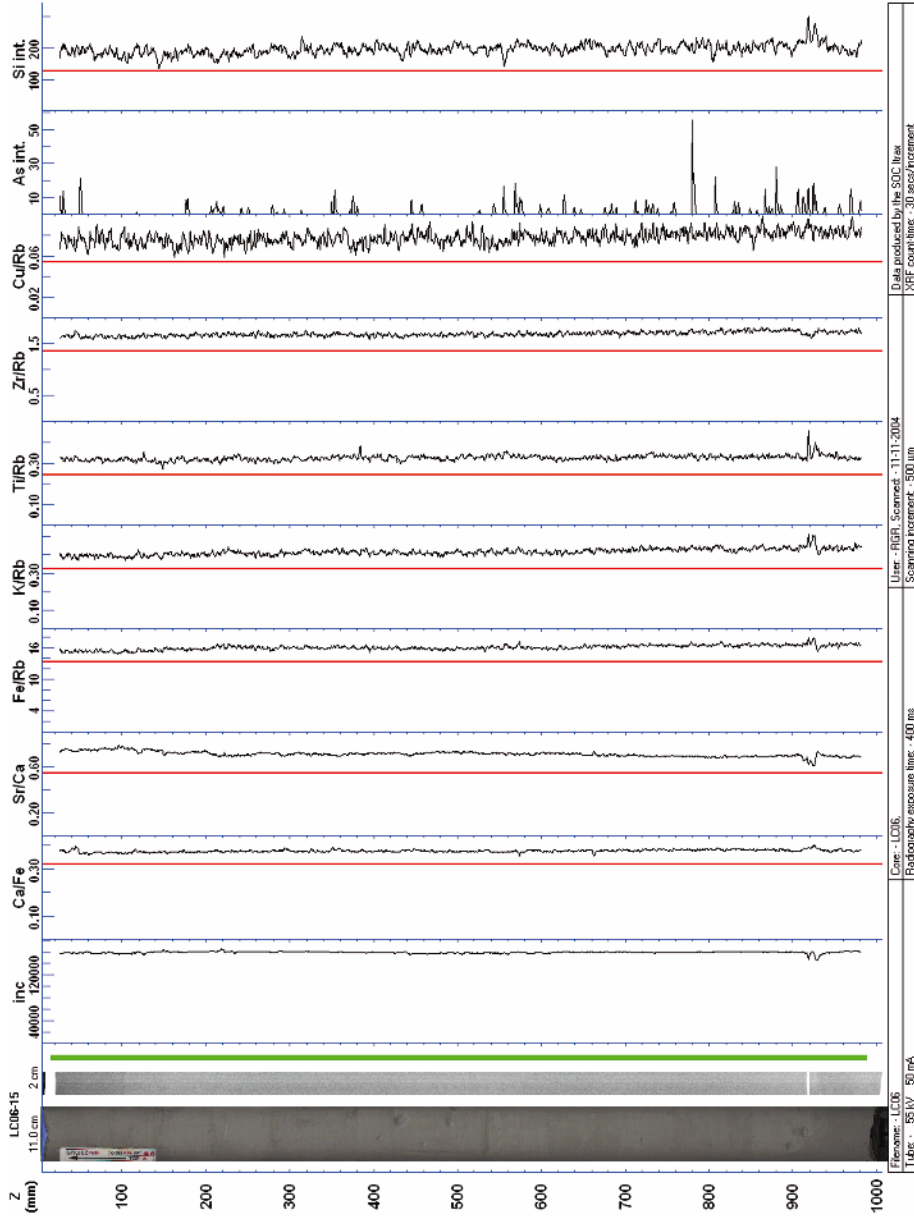


Fig. 6. Compton scattering and downcore geochemical profiles through LC06 Section 15 (14.78–15.78 mbct). See the description of Figures 4 and 5 for a description of the data display. These records are through visually ungraded turbidite mud, part of a 5.5 m-thick megaturbidite deposited 22 ka ago during the last lowstand of sea level (Rothwell *et al.* 1998). Note the slight compositional grading apparent in the ratio profiles, which may reflect increasing clay content towards the top of the core. The variability seen in the Cu/Rb, As and Si profiles reflects the low concentrations of these elements present.

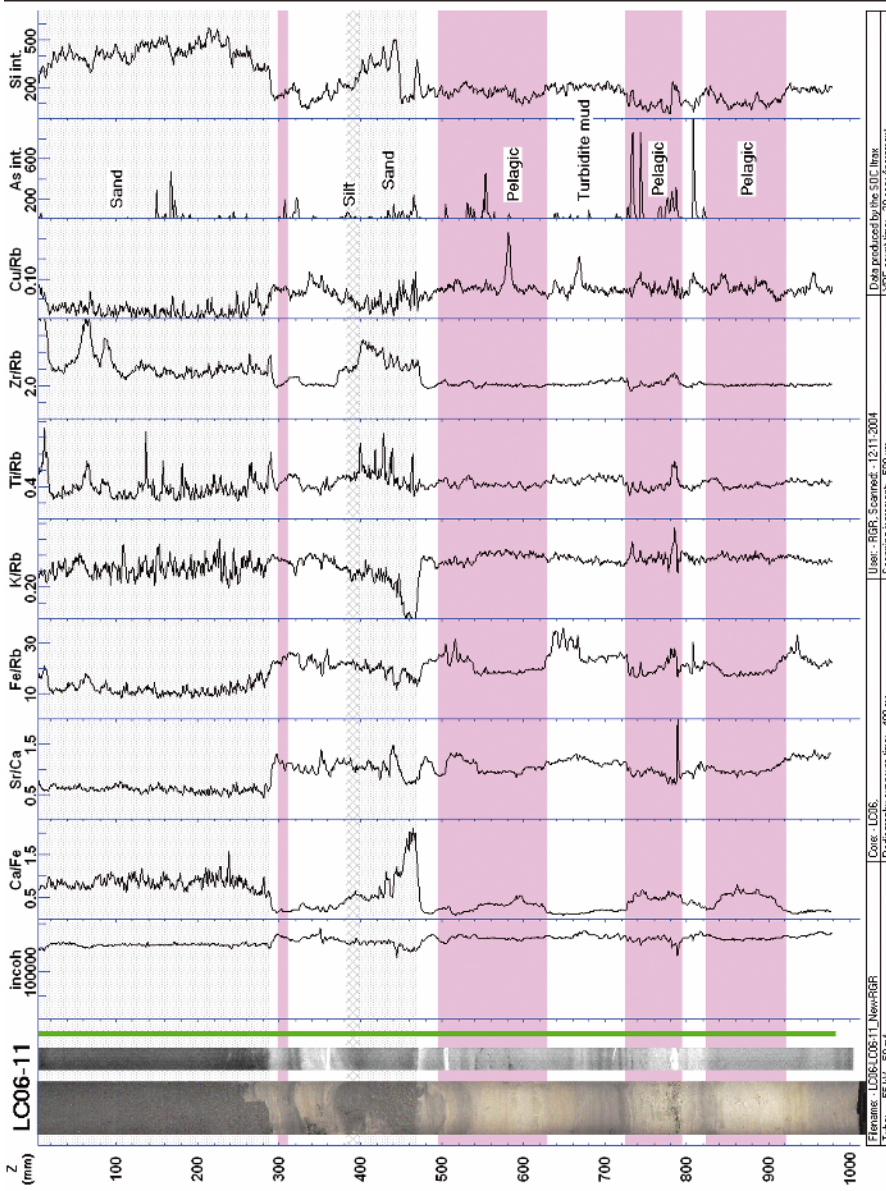


Fig. 7. Compton scattering and downcore geochemical profiles through core section 11 (18.78–19.78 mbct). See the description of Figures 4 and 5 for a description of the data display. White intervals are turbidite mud. The sand at 0–300 mm is the base of the megaturbidite, part of which is displayed in Figure 6. Note the distinctive geochemical character of the turbidite seen at 320–490 mm that is believed to belong to a small group of turbidites with a proximal source. The sharp peak in the Sr/Ca ratio at 790 mm correlates with a thin tightly packed layer of pteropod debris within a pelagic interval, but probably is a sediment fabric/grain-size/shape-related feature rather than a true compositional fluctuation.

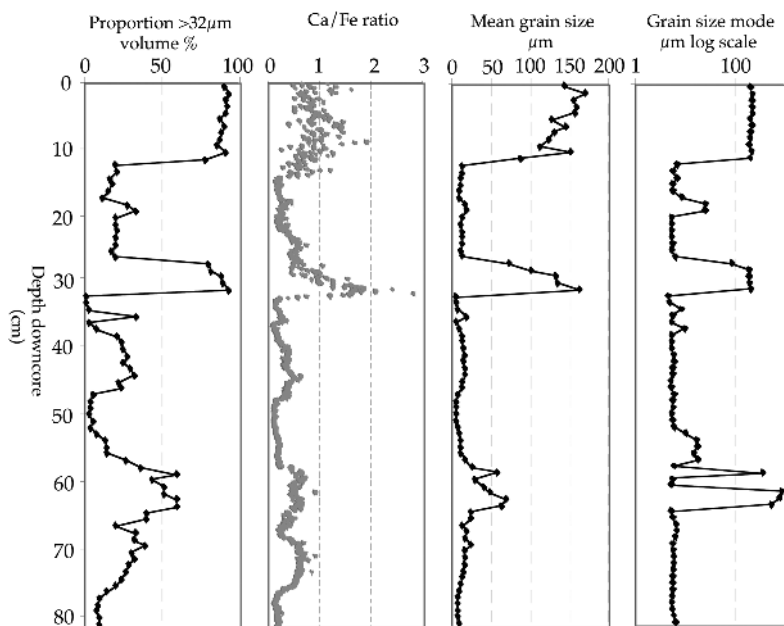


Fig. 8. Grain-size profiles and Ca/Fe ratio through LC06 section 11, 15–97 cm (cf. Fig. 7). Note the close correspondence between the Ca/Fe profile and the mean grain size and the proportion of grains $>32\mu\text{m}$ in the sediment, suggesting that Ca content closely relates to the presence of foraminifers. The Ca/Fe ratio seems a good proxy for textural variation. Grain-size measurement was made at a resolution of 1 cm over the interval studied.

Ca/Fe profile shape within turbidites appears to mirror grading, or its absence (Fig. 8), and provide clear indication of the Piper (1978) and Stow & Shanmugam (1980) textural subdivisions without the need for grain-size analysis. Bioturbative mixing of pelagite into the upper parts of turbidites causes the Ca/Fe ratio to decrease in the tops of the turbidite units. Identification of textural subdivisions is important in assessing source distality–proximity relationships. Calcium peaks, or lack of Ca peaks (commonly associated with increased Si), within turbidite bases distinguish foraminifer- or shell-rich and more terrigenous quartz-rich bases. A small number of turbidites with sandy bases have relatively higher Ca and lower Fe compared to the others, and may have a more proximal source. The Ca/Fe profile within pelagites is typically more variable than in turbidites, reflecting the more heterogeneous bioturbated sediment fabric (Fig. 8).

Sr/Ca ratio. Biogenic low-Mg calcite from surface ocean production has a limited Sr/Ca range (e.g. 1100 and 1900 $\mu\text{g Sr g}^{-1} \text{CaCO}_3$ in foraminifer and coccolith calcites according to Stoll & Schrag 2000) and enhanced Sr may indicate

the presence of high-Sr aragonite, which requires a shallow-water source (Thomson *et al.* 2004). Shallow and lagoonal waters on subtropical and temperate continental shelves are commonly rich in *Halimeda* (a macroscopic green calcareous algae whose calcified segments are composed of very fine-grained aragonite). *Halimeda*-rich sediments are described from shallow temperate bays along Mediterranean coastlines (e.g. Fornos *et al.* 1992; Hieke & Werner 2000). Where it occurs *Halimeda* is an important contributor to neritic sediments. Many neritic invertebrates, such as bivalves, gastropods and corals, have aragonitic shells. Hence, neritic carbonate debris is richer in aragonite than ocean productivity derived low-Mg calcite of foraminifera and coccoliths, so the Sr/Ca ratio may reflect provenance. Turbidites with sandy bases, apart from the megabed (13.5–19 mbct, Fig. 3), generally show higher Sr/Ca values than turbidites lacking coarse-grained bases, perhaps indicating a different, more proximal provenance (e.g. North African or Sardinian shelf). The Sr/Ca ratio, however, like the other parameters measured, is affected by sediment-packing/porosity and grain-size/shape variations. Pelagic intervals containing abundant pteropods commonly register high

Sr/Ca, although pteropod shells are composed of low-Sr aragonite (Krinsley & Bieri 1959; Kinsman 1969; Rutten *et al.* 2000) so, in these cases, the high Sr/Ca values must be a texturally related effect (Fig. 7).

Fe/Rb ratio. The Fe/Rb ratio, like Sr/Ca, also commonly shows grain-size-related fractionation effects within turbidites. Fe is mobilized during redox-related diagenesis, so elevated Fe contents are seen within bioturbated (formerly oxidized) parts of turbidites that have been affected by post-deposition oxidation by bottom-water O₂ diffusion into the turbidite after emplacement (e.g. section 11, 62.5–67 and 91.5–95 cm, Fig. 7). Increased Rb within turbidite muds reflects greater clay contribution to the sediment.

K/Rb ratio. The K/Rb ratio commonly shows low values in silts and sands compared to mud intervals reflecting the presence of K (like Rb) in clays and porosity-related artefacts associated with sea-water Cl absorbing potassium X-rays (Croudace *et al.* 2006).

Zr/Rb and Ti/Rb ratios. Zirconium and Ti contents are high in heavy resistate (i.e. resistant to chemical and mechanical erosion) minerals (de Meijer 1998) and these accessory minerals are commonly enriched in the bases of some turbidites due to gravitative settling. Differences seen in different turbidite bases may reflect distance from sediment source and provenance differences. In Figure 5, the thin silt turbidite between 38 and 41 cm has a lower Zr content than the overlying sand at 29–38 cm, but is very similar to the overlying graded silt at 16–29 cm. The silt bed at 38–41 cm may, therefore, be an early arrival of the overlying graded turbidite at 6–38 cm (see discussion below).

Cu/Rb. The behaviour of Cu in marine sediments is poorly understood. The Cu/Rb profile shows great variability with Cu peaks, apparently largely of diagenetic origin, occurring in both pelagic and turbidite intervals (e.g. Fig. 7). We believe that the discreet nature of the peaks discounts the possibility of any Cu artefact significantly affecting the data.

As. Arsenic is efficiently excited using a Mo tube, so that coherent As signals are seen with the ITRAX even at low concentrations. Arsenic may be present as a detrital or authigenic phase and commonly indicates the presence of pyrite (FeS₂). Indeed, As is a better indicator of this mineral than Fe, due to high background levels of Fe in detrital phases making it difficult to distinguish the relatively small additional amounts

of Fe in authigenic pyrite. In contrast, As has a low concentration in detrital phases but a high concentration in pyrite. Pyrite occurs in a wide range of grain sizes. Authigenic pyrite is widespread in marine sediments and can form in localized microenvironments where oxygen depletion and sulphate reduction occurs, such as within burrows and foraminifer test chambers. In core LC06 the As integral profiles suggests that detrital pyrite, seen within turbidite bases, is commonly of restricted grain size and more abundant in turbidite silts than sands (e.g. Fig. 5, 15–41 cm). This suggests either that sand-sized pyrite has settled out more proximally, or that the pyrite present is of restricted grain size, perhaps occurring mainly as framboids (spheroidal grains composed of pyrite microcrystallites), the most common form of pyrite in marine sediments, formed by sulphate reduction within microfossil tests.

Br/Cl. Bromine contents are high in organic-rich sediments (Ten Haven *et al.* 1987; also fig. 4 in Thomson *et al.* 2006) causing the Br/Cl ratio to increase over the constant sea-water value. No organic-rich layers were identified in core LC06, however, and Br/Cl ratios are consistently low in all sections.

ITRAX applications and limitations

ITRAX-acquired geochemical data are essentially semi-quantitative in nature and need to be interpreted with caution. Errors may arise due to poor peak discrimination in the X-ray spectra, porosity changes, compaction or grain-size/shape-related artefacts (recorded for K and Sr), low count rates and crack-related effects. Invalid data may be recorded when the X-ray detector is not in the correct position, particularly when the cut core surface is uneven or shows sudden variability. Careful study of variation in the element integral profiles, the Compton scatter integral and the detector–sediment distance index can aid in identifying invalid data. The data visualization program Itrax.PLOT can temporarily remove these suspect data prior to final presentation; the original data are never modified. The ITRAX profiles do allow useful primary textural- and depositional-related and secondary diagenetic features to be identified and their character studied in unprecedented detail.

Early arrivals

A further application of the ITRAX data may be in the identification of turbidite early arrivals.

Early arrivals represent portions of a turbidity current that reach the point of deposition earlier than the main flow, usually due to flow division on the slope or rise. Such division may occur where canyons or channels divide or there is canyon overspill. Early arrival deposits are well documented from deep-sea basins (e.g. Weaver & Rothwell 1987) and commonly appear as basal silts and sands with thin mud caps, which are then directly overlain by the sand and/or silt of the main flow. The sand and silts of the early arrival and the main flow are usually very similar in composition. Several possible early arrivals were identified during visual logging of core LC06 on the basis of textural and colour similarities to the overlying turbidite. However, the ITRAX data showed that in many cases there were significant geochemical differences in the presumed early arrivals and overlying turbidites, possibly because the element/Rb values are different in different grain-size classes. It may be that some early arrivals had entrained other material on their passage downslope or, rather than being early arrivals, some beds may have different sources, representing distinct separate events. Comparison of element/Rb values in some 'early arrival' silts with those in the silts above overlying sands, however, did suggest some beds were probably related to the same turbidity current flow.

Climatic modulation

Identification of individual turbidites, through visual and ITRAX logging, and placing them in a time stratigraphic framework allows assessment of any climatic modulation of emplacement (Fig. 9). This shows that turbidite emplacement at the LC06 core site has varied markedly with time over the last 50 ka, with a significantly increased frequency of turbidite emplacement after 20 ka. Thouveny *et al.* (2000) demonstrated through magnetic susceptibility measurements of sediment fabric and sedimentation rate studies of Calypso piston cores that the upper 10–15 m of some, if not all, Calypso cores are up to 1.5–2 times longer than the same sequence recovered by conventional piston cores on the same site. This is interpreted as being due to syringing or oversampling of the sediments in the upper portion of these long cores due to cable rebound resulting in upward piston acceleration and a microfabric rotation into the vertical during the coring process. Skinner & McCave (2003) also show that the upper 5–15 m of Calypso piston cores are affected by such oversampling on soil mechanics considerations. Turbidites within the upper 20 m of the sediment sequence in core

LC06 are much thicker than those below this level (fig. 3 in Rothwell *et al.* 1998). Further, the time-stratigraphic framework suggests significant stretching of pelagic intervals within this part of the sequence. Uncorrected average pelagic accumulation rates are 11 cm ka^{-1} between 0 and 3.5 mbct, 8 cm ka^{-1} between 3.5 and 13.5 mbct, and approximately 1 cm ka^{-1} below 13.5 mbct. Therefore, stretching of the sequence is implicit over the interval 0–15 mbct. This stretching does not, however, negate the increase in turbidite frequency seen within the upper 20 m of the sequence.

In Figure 9 turbidite thickness and basal sand/silt content are plotted against estimated emplacement time (see the Methods section for method of calculation). The times of emplacement for turbidites above the AMS radiocarbon datum of 8.4 ka are maximum ages only as it is unknown how much of the most recent sediment was lost during the coring process. It is apparent from the figure that the full and Late Glacial of the Late Devensian glaciation and the post-glacial rise in sea level were significant times for turbidite emplacement. Between 26 and 45 ka turbidite emplacement at the LC06 core site was rare with a frequency of one event every 8–9 ka, so that only three thin (from 2 to 11 cm in thickness) mud turbidites were emplaced over this 19 ka time span. The full glacial (26–14 ka) saw a marked increase in both frequency and magnitude of turbidite deposition. During this 12 ka period, 18 turbidites (from >1 to 555 cm in thickness) were deposited with a frequency of one event every 600–700 years, although emplacement frequency increases towards the Late Glacial (Fig. 9). The thickest turbidite present in LC06 was deposited at the Late Glacial Maximum at 22 000 years BP. This 5.5 m-thick bed is a megaturbidite of basin-wide extent that can be mapped as a conspicuous acoustically transparent layer on high-resolution seismic profiles (Rothwell *et al.* 1998). This bed, previously described from five long piston cores and high-resolution seismic profiles across the abyssal plain from as far west as $5^{\circ}30'E$ and as far north as $41^{\circ}10'N$, has a massive sandy base that thickens and coarsens towards the north, suggesting a source on the southern European margin (Rothwell *et al.* 1998). All turbidites with silty and/or sandy bases in core LC06 were emplaced during full or Late Glacial times (Fig. 9). During the Younger Dryas and Holocene (14–0 ka) there was frequent emplacement of mud turbidites. During this time interval 26 turbidites are recorded in LCO6, giving an emplacement frequency of one event approximately every 500 years. The magnitude of Holocene turbidites

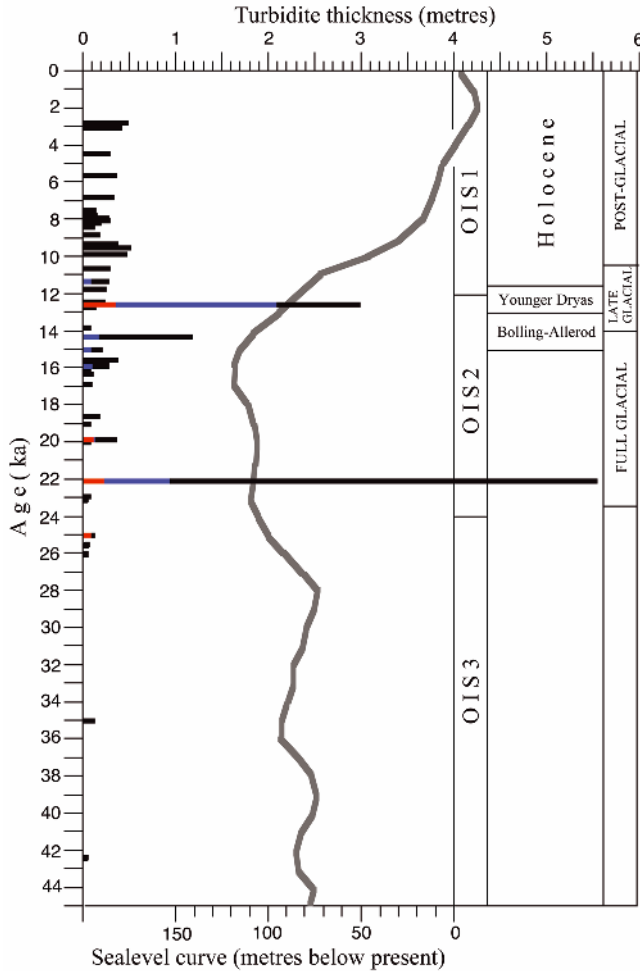


Fig. 9. Emplacement time and bed thickness for turbidites identified in core LC06, 0–20 mbct. Black bars indicate individual mud turbidites, with blue and red bars indicating the thickness of silt and sand, respectively, within turbidite bases, where present. The sea-level curve of Shackleton (1987), and oxygen isotope and climatic boundaries are also shown. Dates for the Younger Dryas and Bolling/Allerod are taken from Hugen *et al.* (2000). Note that emplacement of sand and silt-based turbidites is largely confined to Oxygen Isotope Stage 2 and that frequency of turbidite emplacement strongly correlates to sea-level change, emplacement being most frequent when the rate of sea-level rise is greatest (during the early post-glacial).

is difficult to assess as their thicknesses recorded in the core are clearly stretched. Overall, it seems clear that turbidite emplacement frequency has increased during the Holocene, but that emplacement was most frequent when the rate of change (i.e. rise) of sea level was greatest (Fig. 9). A similar relationship has been reported for the recent and more distant geological record in aseismic areas. Wynn *et al.* (2002), for example, showed that turbidites within the Moroccan Turbidite system (NE Atlantic) were emplaced at Oxygen Isotope Stage boundaries during periods of

rapid sea-level change. Marjanac (1996) attributed the deposition of large turbidites in the Eocene–Miocene flysch of central Dalmatia (Croatia) to periods of sea-level rise. Turbidites on the Madeira Abyssal in the NE Atlantic are also reported to have been emplaced at Marine Isotope Stage boundaries at times of sea-level change (Weaver & Kuijpers 1983; Weaver *et al.* 1992). In the present study, low sea level seems to have been particularly important for the emplacement of large-volume turbidites (assuming thickness correlates with volume in this

depositional setting), but increased turbidite emplacement frequency is essentially a Late Glacial–post-glacial phenomenon.

Turbidite internal subdivisions

Most of the turbidites cored in the sequence are highly distal, many consisting entirely of ungraded E3 (Piper 1978) or T7–T8 mud (Stow & Shanmugam 1980). Indeed, the ITRAX geochemical profiles often provide an excellent proxy for determining grading within turbidite muds (Fig. 8) and identification of their textural subdivision according to the Piper and/or Stow and Shanmugam scheme, for example, allowing discrimination of graded and ungraded mud. In this way ungraded E3 and T7–T8 muds can be distinguished from graded E2 (Piper 1978) or T6 mud (Stow & Shanmugam 1980), a distinction that cannot be made with the human eye. The ITRAX data therefore allow the distality of individual turbidites to be assessed.

Source of turbidites

The pattern of allochthonous sedimentation seen at the LC06 core site suggests that climate and sea-level change are important, even dominant, factors both in affecting turbidite emplacement frequency and the deposition of large-volume beds. The core site is only 100 km distant from the North African margin. The Algerian margin is steep (slopes are 15° or more), incised by canyons (Rehault *et al.* 1985; Déverchère *et al.* 2005) and the hinterland mountainous. The African–Eurasian plate boundary runs in an east–west direction close to the Algerian margin. The African plate moves to the north towards the Eurasian plate in a NNW direction with a translation to the east resulting in seismogenic strike-slip faulting along the margin (Thomas 1976). Large offshore earthquakes on the continental shelf and slope have occurred (Ambraseys 1982; Harbi *et al.* 1999). Some historical earthquakes on the Algerian coast have been destructive. Over 95 earthquakes (including 47 with $M > 5$) have been recorded in NE coastal Algeria (between 35° and 38°N, 4°–9°30') since 1357 AD (Harbi *et al.* 1999, fig. 2). The main river discharging on the eastern Algerian margin is the River Soumam which enters the Gulf of Bejaia, 200 km west of Annaba. The thick sedimentary accumulation offshore of the river mouth is affected by faulting which has generated submarine landslides moving sediments to the basin through the Bejaia Canyon (Harbi 1996; Harbi *et al.* 1999). One submarine earthquake on 21 August 1956 caused a tsunami

along the coast of Jijeli on the eastern coast of the Gulf of Bejaia (Rothé 1950). Seismicity and oversteepening of the shelf edge seawards of river mouths have long been held as potential triggers for turbidity currents. However, there seems little evidence for emplacement of southerly derived turbidites initiated by seismicity or shelf oversteepening at the LC06 core site – a surprising finding considering the known seismicity of the Algerian margin. This suggests that either few turbidites have been generated from the adjacent parts of the Algerian shelf and slope or that they have largely bypassed the LC06 core site. The water depth at the LC06 core site is 15 m less than that recorded in the central Balearic Abyssal Plain (Rothwell 1995) and turbidity current pathways to the deep basin may bypass the LC06 location.

Sand-based turbidites are generally rare in the sediment sequence – only four turbidites with sandy bases are recorded and all were emplaced during the full or Late Glacial. One of these is the basinwide megaturbidite identified by Rothwell *et al.* (1998), known to have a northern provenance. The other three show generally higher Sr/Ca ratios (although this may be a size-fraction effect) than the other turbidites and the geochemistry/mineralogy of the sands (typically high Ca, low Fe and, sometimes, increasing Si towards the base, and commonly containing rare to common rounded hematitic quartz) suggests a local shelf source. Potential sources for turbidites at core site LC06 are varied and include the southern European margin, Balearic Rise, Algerian shelf and slope, and the Sardinian margin. However, the paucity of proximal sandy turbidites with a neritic geochemical signature suggests that any locally derived allochthonous contribution to LC06 is small.

Conclusions

- The ITRAX core scanner provides rapid and non-destructive characterization of downcore geochemical distributions in unprecedented detail along with visual and X-radiographic images. Such data when gathered from turbidite-bearing sequences can provide significant information on grading and bioturbative mixing of turbidites, allow identification of geochemically distinctive marker beds, give indications of differences in provenance between beds, and confirm or query the presence of early arrivals. In the sediment sequence studied, variations in Ca/Fe generally provide a suitable proxy for the occurrence of pelagites and turbidites, allowing

discrimination of genetic units, if this parameter is coupled with others. This, together with a chronostratigraphic framework based on AMS radiocarbon dating and indirect correlation with oxygen isotope stages, demonstrates the dominance of climatic modulation of turbidite deposition in this area, despite proximity of a seismically active continental margin to the south.

- Grading in the Ca/Fe ratio within turbidite beds closely mirrors textural grading and allows discrimination of graded and ungraded turbidite muds without the need for grain-size determinations. Identification of fine texturally related detail, which may be invisible to the naked eye, suggests ITRAX data may allow assessment of turbidite distality in cored sequences and observations on the proximity of source areas.
- Semi-quantitative high-resolution geochemical profiling using the ITRAX micro-XRF core scanner has identified a few turbidite beds with distinctive geochemistry and these are potential marker beds for correlative purposes if found in other Balearic Abyssal Plain cores. The ITRAX micro-XRF core scanner data also provide useful information to confirm or query beds postulated as early arrivals of overlying turbidites.
- High-resolution geochemical profiling through sediment sequences containing turbidite beds provides a wealth of detailed geochemical information related to texture, mixing, provenance and diagenesis. These data need to be interpreted with caution and from an informed standpoint, however. Artefacts related to porosity, compaction and grain-size/shape changes, unevenness of the cut core surface, poor discrimination of close element peaks or instrument sensitivity issues relating to particular elements can complicate interpretation. The ITRAX data as presently recorded are best viewed as semi-quantitative in nature, and more studies are needed to compare and calibrate the records obtained with those measured using traditional destructive analysis (XRF or ICP-OES).
- Deposition of sand and/or silt-based turbidites on the SE Balearic Abyssal Plain during the last 50 ka is restricted to the full and Late Glacial. The thickest (largest volume) turbidites are also emplaced at this time. Turbidite emplacement frequency increases during the Holocene and is most frequent when the rate of post-glacial sea-level rise is greatest.
- Proximal turbidites with a southerly (Algerian margin) or northeasterly source (Sardinian

margin) are rare at the LC06 core site. Such turbidites, some perhaps seismically initiated, may bypass this location to reach the deeper parts of the Balearic Basin.

The authors are very grateful to Drs A. Cattaneo and T. Courp for their reviews that significantly improved the paper. Professor P. Weaver is thanked for his editorial handling of the manuscript.

References

- AMBRASEYS, N.N. 1982. The seismicity of North Africa: the earthquake of 1856 at Jijeli, Algeria. *Bollettino di Geofisica e Teorica ed Applicata*, **24**, 31–37.
- BOUMA, A.H. 1962. *Sedimentology of Some Flysch Deposits*. Elsevier, Amsterdam.
- CROUDACE, I.W., RINDBY, A. & ROTHWELL, R.G. 2006. ITRAX: description and evaluation of a new multi-function X-ray core scanner. In: ROTHWELL, R.G. (ed.) *New Techniques in Sediment Core Analysis*. Geological Society, London, Special Publications, **267**, 51–63.
- DE MEIJER, R.J. 1998. Heavy minerals: from 'Edelstein' to Einstein. *Journal of Geochemical Exploration*, **62**, 81–103.
- DÉVERCHÈRE, J., YELLES, K. *ET AL.* 2005. Active thrust faulting offshore Boumerdes, Algeria, and its relations to the 2003 Mw 6.9 earthquake. *Geophysical Research Letters*, **32**, L04311, doi:10.1029/2004GL021646.
- FORNOS, J.J., FORTEZA, V., JAUME, C. & MARTINEZ-TABERNER, A. 1992. Present-day *Halimeda* carbonate sediments in temperate Mediterranean embayments: Fornells, Balearic Islands. *Sedimentary Geology*, **75**, 283–293.
- HARBI, A. 1996. *La marge algérienne orientale: resultants d'une étude par sismique réflexion*. C.R.A.A.G Publications (internal report), Algeria, **762**.
- HARBI, A., MAUCHE, S. & AYADI, A. 1999. Neotectonics and associate seismicity in the Eastern Tellian Atlas of Algeria. *Journal of Seismology*, **3**, 95–104.
- HASCHKE, M. 2006. The Eagle III BKA system, a novel sediment core X-ray fluorescence analyser with very high spatial resolution. In: ROTHWELL, R.G. (ed.) *New Techniques in Sediment Core Analysis*. Geological Society, London, Special Publications, **267**, 31–37.
- HAUG, G.H., HUGHEN, K.A., SIGMAN, D.M., PETERSON, L.C. & RÖHL, U. 2001. Southward migration of the Intertropical Convergence Zone through the Holocene. *Science*, **293**, 1304–1308.
- HIEKE, W. & WERNER, F. 2000. The Augias megaturbidite in the central Ionian Sea (central Mediterranean) and its relation to the Holocene Santorini event. *Sedimentary Geology*, **135**, 205–218.
- HOOGAKKER, B.A.A. 2003. *Climate control of allochthonous sedimentation in the deep sea*. PhD thesis, University of Southampton.
- HUGHEN, K.A., SOUTHON, J.R., LEHMAN, S.J. & OVERPECK, J.T. 2000. Synchronous radiocarbon and climate shifts during the last deglaciation. *Science*, **290**, 1951–1954.

- JAHN, B., DONNER, B., MÜLLER, P.J., RÖHL, U., SCHNEIDER, R. & WEFER, G. 2003. Pleistocene variations in dust input and marine productivity in the northern Benguela Current: evidence of evolution of global glacial–interglacial cycles. *Palaeogeography, Palaeoclimatology, Palaeoecology*, **193**, 515–533.
- JANSEN, J.H.F., VAN DER GAAST, S.J., KOSTER, B. & VAARS, A.J. 1998. CORTEX, a shipboard XRF-scanner for element analyses in split sediment cores. *Marine Geology*, **151**, 143–153.
- KINSMAN, D.J.J. 1969. Interpretation of Sr²⁺ concentrations in carbonate minerals and rocks. *Journal of Sedimentary Petrology*, **39**, 486–507.
- KRINSLEY, D. & BIERI, R. 1959. Changes in the chemical composition of pteropod shells after deposition on the sea floor. *Journal of Paleontology*, **33**, 682–684.
- KRUMBEIN, W.C. 1936. Application of logarithmic moments to size frequency distributions of sediments. *Journal of Sedimentary Petrology*, **6**, 35–47.
- KUHLMANN, H., FREUDENTHAL, T., HELMKE, P. & MEGGERS, H. 2004. Reconstruction of paleoceanography off NW Africa for the last 40,000 years: influence of local and regional factors on sediment accumulation. *Marine Geology*, **207**, 209–234.
- LAMY, F., KAISER, J., NINNEMANN, U., HEBBELN, D., ARZ, H.W. & STONER, J. 2004. Antarctic timing of surface water changes off Chile and Patagonian ice-sheet response. *Science*, **304**, 1959–1962.
- LAJ, C., MAZAUD, A. & DUPLESSY, J.-C. 1996. Geomagnetic intensity and ¹⁴C abundance in the atmosphere and ocean during the past 50 kyr. *Geophysical Research Letters*, **23**, 2045–2048.
- LOWE, D.R. 1982. Sediment gravity flows: II Depositional models with special reference to the deposits of high-density turbidity currents. *Journal of Sedimentary Petrology*, **52**, 279–297.
- MARTINSON, D.G., PISIAS, N.G., HAYES, J.D., IMBRIE, J., MOORE, T.C. & SHACKLETON, N.J. 1987. Age dating and the orbital theory of the ice Ages: Development of a high-resolution 0 to 300,000-year chronostratigraphy. *Quaternary Research*, **27**, 1–29.
- MARJANAC, T. 1996. Deposition of megabeds (megaturbidites) and sealevel change in a proximal part of the Eocene-Miocene flysch of central Dalmatia (Croatia). *Geology*, **24**, 543–546.
- MUTO, T. & STEEL, R.J. 2002. In defense of shelf-edge delta development during falling and lowstand of relative sea level. *Journal of Geology*, **110**, 421–436.
- OCEAN DRILLING PROGRAM. 1987. *Handbook for Shipboard Sedimentologists*. ODP Technical Note, **8**.
- PIPER, D.J.W. 1978. Turbidite muds and silts on deep sea fans and abyssal plains. In: STANLEY, D.J. & KELLING, G. (eds) *Sedimentation in Submarine Canyons, Fans and Trenches*. Hutchison & Ross, Stroudsburg, PA, 163–176.
- POSAMENTIER, H.W. & VAIL, P.R. 1988. Eustatic control on clastic deposition II – sequence and systems tract models. In: WILGUS, C.K., HASTINGS, B.S. *et al.* *Sealevel Changes – An Integrated Approach*. Society of Economic Paleontologists and Mineralogists, Special Publications, **42**, 125–154.
- REHAULT, J.-P., BOILLLOT, G. & MAUFFRET A. 1985. The Western Mediterranean Basin. In: STANLEY, D.J. & WEZEL, F.-C. (eds) *Geological Evolution of the Mediterranean Basin, Raimondo Selli Commemorative Volume*. Springer, Berlin, 101–129.
- RICHTER, T.O., VAN DER GAAST, S. *ET AL.* 2006. The Avaatech XRF Core Scanner: technical description and applications to NE Atlantic sediments. In: ROTHWELL, R.G. (ed.) *New Techniques in Sediment Core Analysis*. Geological Society, London, Special Publications, **267**, 39–50.
- ROLLINSON, H.R. 1993. *Using Geochemical Data: Evaluation, Presentation, Interpretation*. Pearson Education, Upper Saddle River, NJ.
- ROTHÉ, J.P. 1950. *Les séismes de Kherrata et la sismicité de l'Algérie*. Publication Service, Cartes Géologique de l'Algérie, **4**, 1–40.
- ROTHWELL, R.G. (ed.). 1995. *Cruise Report: Marion Dufresne Cruise 81. Mediterranean Giant Piston Coring Transect*. National Oceanographic Library, National Oceanography Centre, Southampton, UK. Unpublished report.
- ROTHWELL, R.G., PEARCE, T.J. & WEAVER, P.P.E. 1992. Late Quaternary evolution of the Madeira Abyssal Plain, Canary Basin. *Basin Research*, **4**, 103–131.
- ROTHWELL, R.G., THOMSON, J. & KÄHLER, G. 1998. Low sealevel emplacement of a very large Late Pleistocene megaturbidite in the western Mediterranean Sea. *Nature*, **392**, 377–380.
- ROTHWELL, R.G., WEAVER, P.P.E., HODKINSON, R.A., PRATT, C.E., STYZEN, M.J. & HIGGS, N.C. 1994. Clayey nannofossil ooze turbidites and hemipelagites at Sites 834 and 835 (Lau Basin, Southwest Pacific). In: HAWKINS, J., PARSON, L. ALLAN, J. *ET AL.* *Proceedings of the Ocean Drilling Program*, **135**, 101–130.
- RUTTEN, A., DE LANGE, G.J., ZIVERI, P., THOMSON, J., VAN SANTVOORT, P.J.M., COLLEY, S. & CORSELLI, C. 2000. Recent terrestrial and carbonate fluxes in the pelagic eastern Mediterranean; a comparison between sediment trap and surface sediment. *Palaeogeography, Palaeoclimatology and Palaeoecology*, **158**, 197–213.
- SHACKLETON, N.J. 1987. Oxygen isotopes, ice volume and sea level. *Quaternary Science Reviews*, **6**, 183–190.
- SHANMUGAM, G. & MOIOLA, R.J. 1982. Eustatic control of turbidite deposition and winnowed turbidites. *Geology*, **10**, 231–235.
- SHANMUGAM, G. & MOIOLA, R.J. 1984. Eustatic control of calciclastic turbidites. *Marine Geology*, **56**, 273–278.
- SKINNER, L.C. & McCAVE, I.N. 2003. Analysis and modelling of gravity- and piston coring based on soil mechanics. *Marine Geology*, **199**, 181–204.
- STOLL, H.M. & SCHRAG, D.P. 2000. Coccolith Sr/Ca as a new indicator for coccolithophorid calcification and growth rate. *Geochemistry, Geophysics and Geosystems*, **1**, paper 1999GC000015 (<http://www.agu.org/pubs/crossref/2000.../1999GC000015.shtml>; date of citation 25.2.05).
- STOW, D.A.V. & SHANMUGAM, G. 1980. Sequence of structures in fine-grained turbidites: comparison

- of recent deep sea and ancient flysch sediments. *Sedimentary Geology*, **25**, 23–42.
- STUIVER, M., REIMER, P.J. *ET AL.* 1998. INTCAL98 radiocarbon age calibration 24,000–0 cal BP. *Radiocarbon*, **40**, 1041–1083.
- TEN HAVEN, H.L., DE LEEUW, J.W., SCHENK, P.A. & KLAVER, G.T. 1987. Geochemistry of Mediterranean sediments: Bromine/organic carbon and uranium/organic carbon ratios as indicators for different sources of input and post-depositional oxidation respectively. *Organic Geochemistry*, **13**, 255–261.
- THOMAS, G. 1976. Mise en évidence de décrochements dextre Est–Ouest d’âge Quaternaire en Algérie Nord Occidentale. *Comptes Rendues de l’Academie des Sciences, Paris*, **283**, 893–896.
- THOMSON, J., CROUDACE, I.W. & ROTHWELL, R.G. 2006. A geochemical application of the ITRAX scanner to a sediment core containing eastern Mediterranean sapropel units. In: ROTHWELL, R.G. (ed.) *New Techniques in Sediment Core Analysis*. Geological Society, London, Special Publications, **267**, 65–77.
- THOMSON, J., CRUDELI, D., DE LANGE, G., SLOMP, C.P., ERBA, E., CORSELLI C. & CALVERT, S.E. 2004. *Florisphaera profunda* and the origin and diagenesis of carbonate phases in eastern Mediterranean sapropel units. *Paleoceanography*, **19**, PA3003 doi:10.1029/2003PA000976.
- THOUVENY, N., MORENO, E., DELANGHE, D., CANDON, L., LANCELOT, Y. & SHACKLETON, N.J. 2000. Rock magnetic detection of distal ice-rafted debris: clues for the identification of Heinrich layers on the Portuguese margin. *Earth and Planetary Science Letters*, **180**, 61–75.
- VAIL, P.R., MITCHUM, R.M., JR *ET AL.* 1977. Seismic stratigraphy and global changes in sealevel. In: PAYTON, C.E. (ed.) *Seismic Stratigraphy—Application to Hydrocarbon Exploration*. AAPG Memoir, **26**, 49–212.
- VAN DER WEIJDEN, C.H. 2002. Pitfalls of normalisation of marine geochemical data using a common divisor. *Marine Geology*, **184**, 167–187.
- WEAVER, P.P.E. 1983. An integrated stratigraphy of the upper Quaternary of the Kings Trough flank area, NE Atlantic. *Oceanologica Acta*, **6**, 451–456.
- WEAVER, P.P.E. & KUIJPERS, A. 1983. Climatic control of turbidite deposition on the Madeira Abyssal Plain. *Nature*, **306**, 360–363.
- WEAVER, P.P.E. & ROTHWELL, R.G. 1987. Sedimentation on the Madeira Abyssal Plain over the last 300,000 years. In: WEAVER, P.P.E. & THOMSON, J. (eds) *Geology and Geochemistry of Abyssal Plains*. Geological Society, London, Special Publications, **31**, 71–86.
- WEAVER, P.P.E., ROTHWELL, R.G., EBBING, J., GUNN, D. & HUNTER, P.M. 1992. Correlation, frequency of emplacement and source directions of megaturbidites on the Madeira Abyssal Plain. *Marine Geology*, **109**, 1–20.
- WILSON, T.R.S., THOMSON, J., COLLEY, S., HYDES, D.J., HIGGS, N.C. & SORENSEN, J. 1986. Early organic diagenesis: the significance of progressive subsurface oxidation fronts in pelagic sediments. *Geochimica et Cosmochimica Acta*, **49**, 611–822.
- WYNN, R.B., WEAVER, P.P.E., MASSON, D.G. & STOW, D.A.V. 2002. Turbidite depositional architecture across three interconnected deep-water basins on the northwest African margin. *Sedimentology*, **49**, 669–695.